Journal of Applied Physics

High-temperature photocurrent mechanism of #-Ga_2O_3 based metal-semiconductor-metal solar-blind photodetectors

Cite as: J. Appl. Phys. **125**, 144501 (2019); https://doi.org/10.1063/1.5088532
Submitted: 11 January 2019 . Accepted: 22 March 2019 . Published Online: 08 April 2019

B. R. Tak, Manjari Garg, Sheetal Dewan, Carlos G. Torres-Castanedo, Kuang-Hui Li, Vinay Gupta, Xiaohang Li, and R. Singh

Journal of Applied Physics | ARTICLE | scitation.org/journal/jap

High-temperature photocurrent mechanism of β-Ga_2O_3 based metal-semiconductor-metal solar-blind photodetectors

Cite as: J. Appl. Phys. **125**, 144501 (2019); doi: 10.1063/1.5088532
Submitted: 11 January 2019 · Accepted: 22 March 2019 ·
Published Online: 8 April 2019

B. R. Tak,[1,a)] Manjari Garg,[1] Sheetal Dewan,[2] Carlos G. Torres-Castanedo,[3] Kuang-Hui Li,[3] Vinay Gupta,[2] Xiaohang Li,[3] and R. Singh[1]

AFFILIATIONS

[1]Department of Physics, Indian Institute of Technology Delhi, New Delhi 110016, India
[2]Department of Physics and Astrophysics, University of Delhi, Delhi 110007, India
[3]Advanced Semiconductor Laboratory, King Abdullah University of Science and Technology (KAUST), Thuwal 23955-6900, Saudi Arabia

[a)]Electronic mail: bheraramtak@gmail.com

ABSTRACT

High-temperature operation of metal–semiconductor–metal (MSM) UV photodetectors fabricated on pulsed laser deposited β-Ga_2O_3 thin films has been investigated. These photodetectors were operated up to 250 °C temperature under 255 nm illumination. The photo to dark current ratio of about 7100 was observed at room temperature and 2.3 at a high temperature of 250 °C with 10 V applied bias. A decline in photocurrent was observed until a temperature of 150 °C beyond which it increased with temperature up to 250 °C. The suppression of the UV and blue band was also observed in the normalized spectral response curve above 150 °C temperature. Temperature-dependent rise and decay times of temporal response were analyzed to understand the associated photocurrent mechanism at high temperatures. Electron–phonon interaction and self-trapped holes were found to influence the photoresponse in the devices. The obtained results are encouraging and significant for high-temperature applications of β-Ga_2O_3 MSM deep UV photodetectors.

INTRODUCTION

Deep UV (DUV) photodetectors, also known as solar-blind photodetectors with high thermal stability, have drawn considerable attention due to their wide potential applications in defense, security, space communications, UV astronomy, and biological and environmental studies.[1–5] As the science advances, high-temperature DUV photodetectors will be an important constituent for the aforementioned applications.[5,6] For high-temperature applications, a photodetector must fulfill the requirements of high thermal stability, high chemical stability, high-temperature operation, high electrical tolerance, and high spectral selectivity. Most of the UV photodetectors in commercial applications are based on silicon (Si) due to the well established Si-technology. However, UV photodetectors based on the current Si-based technology possess limitations of high dark current due to narrow bandgap and require Wood's filters.[7] Additionally, heavy cooling systems were also required for traditional Si-photodetectors to achieve promising external quantum efficiency. For high-temperature applications, these photodetectors are unable to function due to their large thermally generated carriers, which leads to negligible photoresponse. In the past few years, wide bandgap semiconductor materials such as AlGaN, SiC, and ZnMgO-based solar-blind photodetectors were explored for operation at elevated temperatures.[8–14] The wide bandgap of these materials was advantageous and eliminated the requirement of Wood's filters. Heavy doping in AlGaN and ZnMgO causes crystalline quality degradation and leads to background signals in the environment.[15,16] The AlGaN/GaN photodetectors were reported at elevated temperatures of 200 °C.[8] However, the photo to dark current ratio (PDCR) (~0.1) and decay time (34 s) at 200 °C was not so impressive. A faster decay time was reported at 200 °C than at room temperature (RT) due to a faster electron–hole recombination process. SiC-based photodetectors possess limitations such as cost

and indirect bandgap, which motivated researchers to search for new materials.[1]

Nowadays, an upsurge in research on β-Ga_2O_3 based DUV photodetectors has been witnessed due to their intrinsic solar-blind nature and high absorption coefficient (>10^5).[17–24] This intrinsic solar-blind nature eliminates the complexity of doping, and thus, β-Ga_2O_3 based DUV photodetectors are more advantageous than AlGaN, SiC, ZnMgO, etc. They also possess eminent thermal and chemical stability, which makes them potential candidates to function in harsh environments.[25,26] However, there are only a few reports available on high-temperature operations of solar-blind photodetectors.[9,27,28] Recently, Ahn *et al.* reported the temperature-dependent PDCR of Si-implanted β-Ga_2O_3 thin films grown by metal organic chemical vapor deposition (MOCVD) with Ti/Au metal contacts.[27,29] They observed a continuous increase in photocurrent with temperature due to the presence of defects in the bandgap. These photodetectors showed a high persistence photocurrent even at RT due to the ohmic behavior of Ti/Au contacts on Ga_2O_3. Wei *et al.* also demonstrated the potential of Ga_2O_3 photodetectors at 427 °C using IZO (In doped ZnO) as a transparent electrode.[30] However, they performed measurements under 185 nm illumination with a very high power density of 14 W/m^2. Also, in the previous reports,[8,27,28,30–32] photoresponse on various high-temperature stable UV photodetectors was shown to either increase or decrease with increase in temperature. The physical mechanism responsible for photoresponse increase or decrease with temperature was not explained. Therefore, the development of solar-blind photodetectors for high-temperature applications is at its early stage and further investigations are needed to understand the physical mechanism of photocurrent transport and persistence photocurrent at high temperatures.

Herein, the high-temperature performance of DUV photodetectors fabricated on Ga_2O_3 thin films was investigated at different temperatures from RT up to 250 °C. The Ga_2O_3 thin films used for fabrication of photodetectors were deposited using the pulsed laser deposition (PLD) technique. X-ray diffraction (XRD) and transmission electron microscopy (TEM) with fast Fourier transform (FFT) were performed to analyze the crystalline quality of as-deposited thin films. A low dark current is desired to obtain a high PDCR. Therefore, the metal–semiconductor–metal (MSM) structure was fabricated with Ni/Au as a Schottky metal contact. Temperature-dependent spectral responsivity, PDCR, and temporal response characteristics of Ga_2O_3 solar-blind photodetectors led to superior operational performance of these photodetectors in harsh environments. The charge carrier transport mechanism across the metal–semiconductor interface is also discussed with respect to spectral and temporal responses, which deepens the understanding of the operation of solar-blind photodetectors at high temperatures. Combined with the cheaper deposition process, the obtained results of Ga_2O_3 solar-blind photodetectors are encouraging and pave the way for the aforementioned high-temperature applications.

EXPERIMENTAL

The Ga_2O_3 thin films used for fabrication of DUV photodetectors were deposited on sapphire (0001) substrates using PLD. The deposition was carried out at a 800 °C substrate temperature. The 200 mJ KrF excimer laser with a 10 Hz frequency was used for the ablation of gallium oxide target. The oxygen pressure was maintained at 5×10^{-4} Torr during the deposition. Further experimental information can be found in Ref. 33. X-ray diffraction (Philips Xpert Pro) having Cu Kα ($\lambda = 1.54$Å) radiation was used for structural investigation of the as-grown Ga_2O_3 thin films. Transmission electron microscopy (TEM) images were recorded using the Titan G^2 80-300 ST system with a line resolution of 0.1 nm.

Furthermore, interdigitated electrodes on Ga_2O_3 thin films were patterned in the Class-100 clean room using the maskless lithography system (Intelligent micropatterning, SF-100). These electrodes were 700 μm long and 50 μm wide with a figure spacing of 50 μm. The metal contacts of Ni (30 nm)/Au (40 nm) were deposited using a thermal evaporation system. A nitrogen purged Xenon lamp (75 W), combined with a computer interfaced monochromator (Bentham TMC-300V), was used for the spectral responsivity measurements. An optical UV Fiber (PCU-1000) was used to direct the monochromatic beam over the device under test (DUT) placed on a high-temperature DC probe station (Ever-Being International Corporation, EB 6). The temperature was controlled using a temperature controller ranging from RT to 300 °C. The power spectrum of the Xenon lamp was acquired using a Thorlabs power meter (PM-100D) and a calibrated Si-photodiode (S-130VC). A Keithley semiconductor parameter analyzer (SCS-4200) was also connected for external biasing. All the photodetector performance measurements were performed at atmospheric condition.

RESULTS AND DISCUSSION

Figure 1(a) depicts the typical X-ray diffraction (XRD) 2θ-scan of the gallium oxide thin film. The peaks marked with a star (*) correspond to the c-plane sapphire substrate. The XRD results revealed that the monoclinic structure of the β-Ga_2O_3 thin film was epitaxially grown in ($\bar{2}01$) plane orientation. Cross-sectional transmission electron microscopy (CS-TEM) and the fast Fourier transform (FFT) measurements were performed to further investigate the crystalline quality and the Ga_2O_3–Al_2O_3 interface, as shown in Figs. 1(b) and 1(c), respectively. The sharp Ga_2O_3–Al_2O_3 interface (<2 nm), as depicted in Fig. 2(b), indicated a very small lattice mismatch, which makes sapphire a preferred substrate for the growth of Ga_2O_3 thin films. The FFT image indicated a good crystalline quality of the Ga_2O_3 thin films.

The scanning electron microscope (SEM) image of the fabricated device is shown in the inset of Fig. 1(d) on a 100 μm scale. The interdigitated MSM structure was fabricated with two back to back Ni/Au Schottky contacts. The MSM photodetectors exhibited low dark current and high speed than photodiodes.[34] The RT dark current of 3×10^{-10} A was obtained even at 10 V bias, as shown in Fig. 2(a). The low dark current was achieved due to back to back Ni/Au Schottky contacts. It was 3–4 times lower than the reported dark current for Ohmic metal contacts on Ga_2O_3.[29,35] The low dark current even at a high applied voltage bias is desirable for superior photodetector performances. Figure 2(b) depicts the variation in photocurrent with temperature. It was observed that the photocurrent variation was lesser than that of the dark current

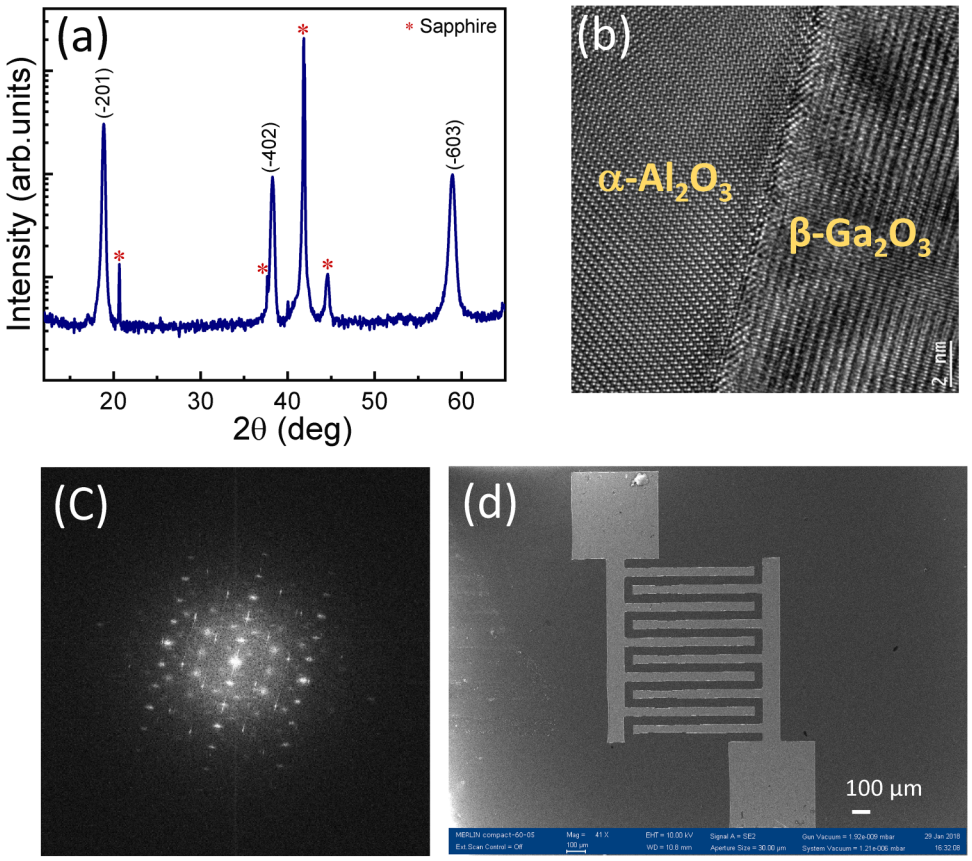

FIG. 1. (a) XRD 2θ scan of a pulsed laser deposited β-Ga_2O_3 thin film. (b) Cross-sectional TEM (CS-TEM) of a Ga_2O_3–Al_2O_3 interface. (c) Fast Fourier transform (FFT) pattern of a β-Ga_2O_3 thin film. (d) SEM image of a fabricated photodetector at 100 μm scale.

with temperature increment. The PDCR ratio is also an essential parameter of photodetectors, which was calculated using the following equation:[36,37]

$$PDCR = \frac{I_p - I_d}{I_d}, \tag{1}$$

where I_p and I_d are denoted as photocurrent and dark current, respectively. The temperature-dependent PDCR is shown in Fig. 3(a). Photocurrent measurements were performed at a 10 V applied bias under 255 nm illumination with a power density of 400 μW/cm^2. It was observed that Ga_2O_3 MSM photodetectors can be used to detect DUV light up to a high temperature of 250 °C

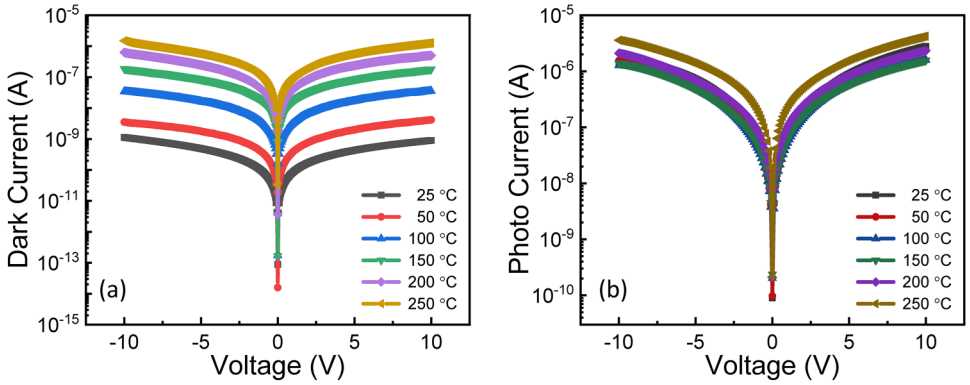

FIG. 2. Variable temperature (a) dark current–voltage and (b) photocurrent–voltage measurement of a Ga_2O_3 photodetector.

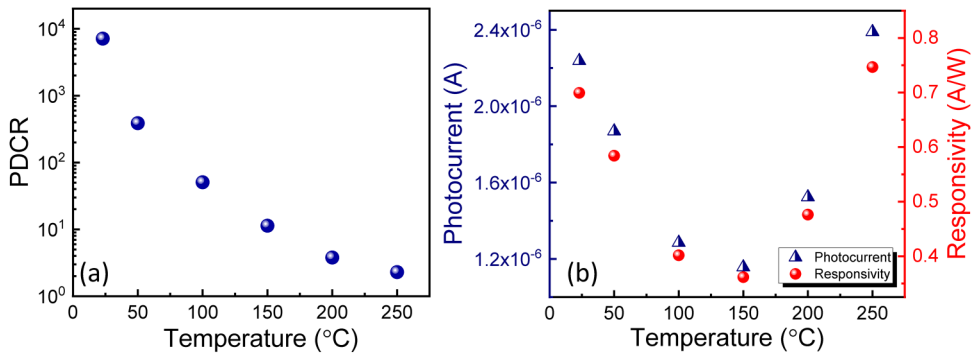

FIG. 3. (a) Temperature-dependent PDCR and (b) photocurrent and peak responsivity of a β-Ga_2O_3 photodetector at 10 V bias and 255 nm illumination.

due to high thermal stability. The PDCR value diminished from 7137 to 2.3 as the temperature was increased from 25 °C to 250 °C. The intrinsic dark current level was again obtained after cooling the device from high temperature to RT, which showed that Ga_2O_3 based Ni/Au MSM DUV photodetectors possess excellent thermal stability. The maximum operating temperature was also higher than that of the AlGaN and nitrogen doped SiC UV detectors.[9,28] Although the Si-doped Ga_2O_3 photodetector showed operation at higher temperatures, it suffered from a high persistence photocurrent even at room temperatures.[29,38] In our case, the high-temperature operation only up to 250 °C was performed due to system limitations. The increased value of the dark current with the temperature led to a decrement in PDCR values due to thermally generated charge carriers.

To analyze the thermal stability at high temperatures, variable temperature photocurrent and responsivity measurements of the fabricated DUV photodetector with 255 nm UV light illumination were analyzed, as shown in Fig. 3(b). Initially, both photocurrent and peak responsivity decreased up to 150 °C, but as the temperature was increased further, both the values started to increase. The responsivity of photodetectors is defined as[39,40]

$$R_\lambda = \frac{I_p - I_d}{PS}, \tag{2}$$

where P is the power density of illuminated light and S is the effective device area, which is 0.008 cm^2 for DUT. The peak responsivity of 0.70 A/W was obtained at RT and it decreased to 0.40 A/W at 150 °C. It increased to 0.74 A/W as the temperature further increased to 250 °C. The decrease in photoresponsivity with temperature was also observed in earlier reports.[28,31,32,41]

The normalized spectral responsivity with varying temperature from RT to 250 °C is depicted in Fig. 4. The spectral responsivity measurements were performed at 10 V applied bias. It can also be observed from the temperature-dependent spectral response that the blue and UV band suppressed as temperature increased. Binet and Gourier also reported similar defect quenching above 400 K.[42] The origin of the UV band in Ga_2O_3 was attributed to a recombination of electrons to self-trapped holes (STHs) and the blue emission was ascribed to a transition between donor and acceptor levels.[42–45] In this report, the suppression of the UV and blue band was observed with increasing temperature from 150 to 250 °C. Hence, the variable temperature spectral response indicated that the STH, as well as the trapped carriers in donor and acceptor states, was no longer stable and became mobile at high temperatures.

The UV/visible discrimination ratio is another important performance parameter of photodetectors. The RT UV (255 nm)/visible (500 nm) discrimination ratio was about 4 orders of magnitude and it decreased to about 2 orders of magnitude at 250 °C. The large UV/visible discrimination ratio at high temperatures assures the practical application of fabricated DUV photodetectors.

The temporal response of MSM photodetectors was investigated to evaluate the detection speed. Time-dependent photocurrent measurements were performed under an illumination of 255 nm wavelength at a 5 V applied bias. The rise and decay time of photocurrent was qualitatively analyzed by fitting the temporal response curve

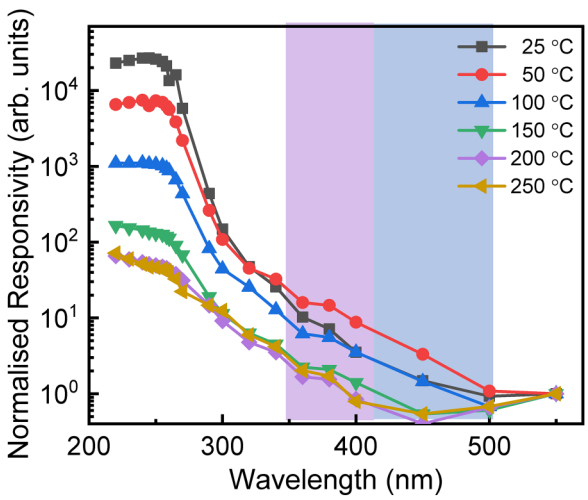

FIG. 4. Spectral response of a fabricated photodetector, with temperature variation ranging from 23 °C to 250 °C.

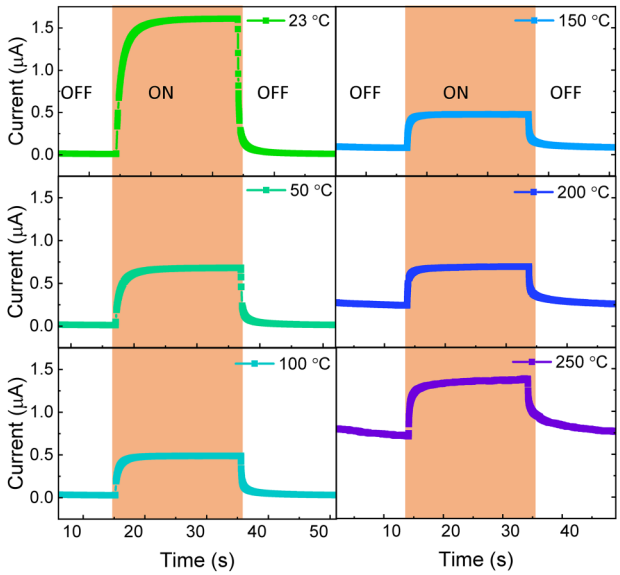

FIG. 5. Real-time current change of a fabricated photodetector at different temperatures under 255 nm UV illumination.

with the following bi-exponential equation:[46,47]

$$I = I_0 + A_1 e^{\frac{-t}{\tau_1}} + A_2 e^{\frac{-t}{\tau_2}}, \tag{3}$$

where I_0 is the steady-state current, τ_1 and τ_2 are the relaxation time constants, and A_1 and A_2 are constants. In general, rise and decay times consist of two components having a fast and a slow response. The fast response component was assigned to change in carrier concentration upon illumination switching. However, the slow response component was attributed to charge carrier trapping/de-trapping influenced by intrinsic defects.[39] Real-time current change under switching ON/OFF of UV light illumination with varying temperature from RT to 250 °C was recorded, as shown in Fig. 5. All of these current pulses were fitted with Eq. (3) and the corresponding rise and decay time constants were obtained, as shown in Fig. 6(a). It was observed that the fast component of decay time (τ_{d1}) remained constant below 150 °C and increased with the rise in temperature further. However, the fast rise time component (τ_{r1}) initially decreased from 590 to 163 ms as the temperature was varied from 25 to 150 °C. Then it slightly increased to 193 ms when the temperature was raised to 250 °C. Evolution of slow components showed that the rise time τ_{r2} decreased from 2.4 to 1.4 s with an increase in temperature from 25 to 150 °C, and then it increased to 3.2 s when the temperature reached 250 °C. However, the slow decay time component τ_{d2}

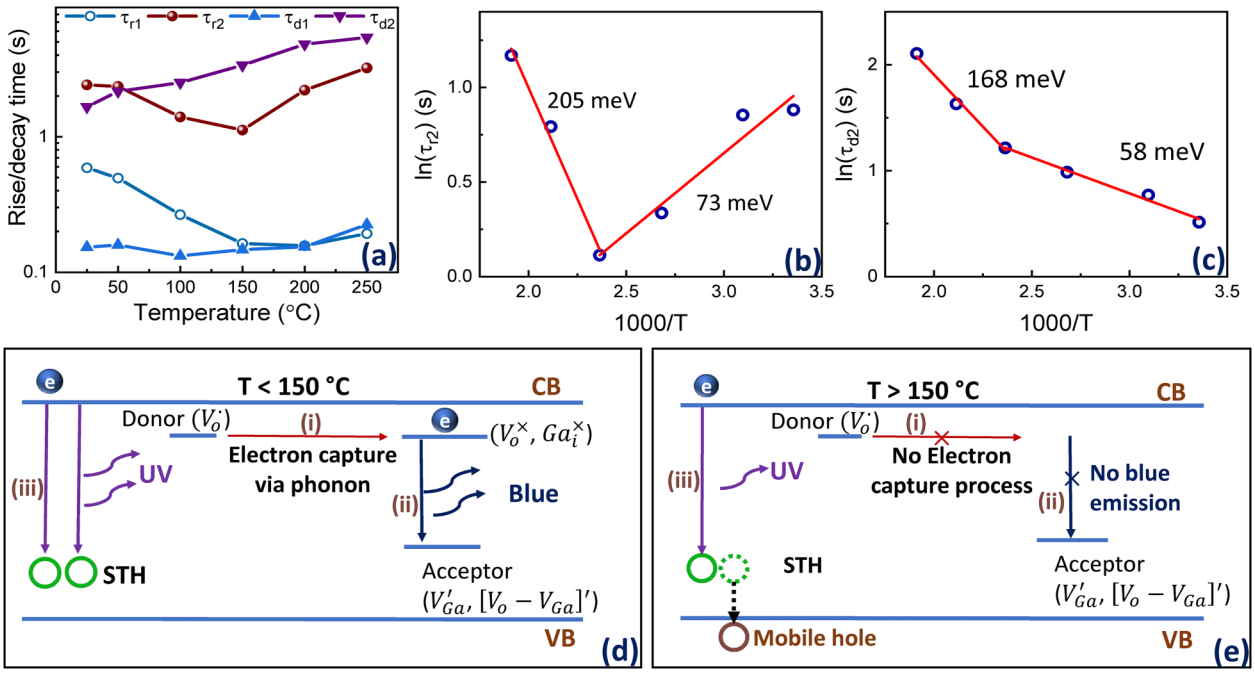

Notations- Dot (·) = Donor, cross (×) = Neutral, prime (′) = Acceptor, V_o = Oxygen vacancy, V_{Ga} = Gallium vacancy, Ga_i= Gallium interstitials, V_o-V_{Ga}= Vacancy complex

FIG. 6. (a) Rise times (τ_{r1} and τ_{r2}) and decay times (τ_{d1} and τ_{d2}) at 5 V bias under 255 nm illumination with detector temperature. (b) Arrhenius plot of slow components of rise times shows activation energies of 73 and 205 meV and (c) decay times depict activation energies of 58 and 168 meV. (d) Model for a photocurrent mechanism below 150 °C, with the electron capture process having activation energies of 58 and 73 meV. (e) Model for a photocurrent mechanism above 150 °C with the transition of STH to a mobile hole having activation energies of 205 and 168 meV.

continuously increased from 1.6 to 5.4 s with a continuous variation of temperature up to 250 °C.

Physical mechanisms of photocurrent transport

As discussed above, the photocurrent and photoresponse decreased with the detector temperature up to 150 °C and increased for higher temperatures (150–250 °C). To understand the physical mechanism of photocurrent generation with temperature, the slow component of the rise time (τ_{r2}) was plotted with 1/T, as depicted in Fig. 6(b).[48,49] The activation energies of 73 and 205 meV were obtained from the linear fit of the Arrhenius plot of the rise time τ_{r2} below and above 150 °C, respectively. Similarly, the slow component of the decay time (τ_{d2}) was plotted with temperature to understand the recombination mechanism, as shown in Fig. 6(c). The two activation energies of 58 meV and 168 meV were obtained below and above 150 °C, respectively. The physical meaning of negative activation energy is related to the carrier generation/recombination ratio.[50] The negative activation energy showed the increasing recombination mechanism and the positive activation energy was attributed to the increasing carrier generation mechanism. The activation energy of 73 meV and 58 meV corresponded to the energy of electron–phonon interactions in Ga_2O_3,[51,52] whereas the activation energy of 205 meV and 168 meV corresponded to the transition of STH to the mobile hole in the valence band.[53]

Binet and Gourier proposed a model for Ga_2O_3 single crystals, which explains the UV and blue emissions.[42] A similar model can be applied here to understand the charge carrier generation/recombination mechanism below and above 150 °C, as shown in Figs. 6(d) and 6(e), respectively. According to this model, three processes occurred during photocurrent transport, labeled as (i), (ii), and (iii), as shown in Fig. 6(d). In process (i), the electron capture from the donor to the neutral defects takes place through phonons, which results in the formation of excitons. The blue emission occurs by a recombination of electrons at the donor to the hole at the acceptor via neutral defects such as $V_o^{\times}$ or $Ga_i^{\times}$, labeled as (ii) in Fig. 6(d). The transition from charged defects to the holes at acceptors was forbidden.[42,43] Process (iii) occurs due to a recombination of conduction band electrons to STH, which results in UV emission. Below 150 °C, all three processes occurred, which led to UV and blue emissions. However, quenching of blue and UV emissions was observed above 150 °C. The quenching of the blue band is possible either by unavailability of electrons at the donor or neutral defects or holes at acceptors. The activation energy of electrons and holes in unintentionally doped β-Ga_2O_3 was reported as about 600 meV and 500 meV, respectively.[54] Therefore, donor electrons and acceptor holes were not de-trapped at the current temperature conditions. Consequently, $V_o^{\times}$ or $Ga_i^{\times}$ was assumed to no longer remain neutral species above 150 °C, which led to the absence of process (i); i.e., no electron capture process. Process (ii) takes place only when process (i) happens. Hence, the blue band got quenched above 150 °C, as shown in Fig. 6(e). The UV emission was also started to suppress above 150 °C due to the transition of STH to the mobile hole in the valence band, which is depicted in Fig. 6(e). Hence, the decrease in photocurrent occurs due to phonon assisted increased carrier trapping in STHs, acceptors, and donors up to 150 °C. Later on, photocurrent increased due to a further decrease in the trap centers.

CONCLUSIONS

In conclusion, high-temperature stability of MSM photodetectors on β-Ga_2O_3 epitaxial films up to 250 °C was demonstrated. The UV/Visible discrimination ratio was as high as 10^4 at RT and 10^2 at 250 °C, which led a high-temperature performance of Ga_2O_3 solar-blind photodetectors. The photoresponsivity initially decreased from RT to 150 °C and then increased with further enhancement in temperature up to 250 °C. The obtained activation energies from the Arrhenius plot of the rise and decay times corresponded to the energy of electron–phonon interaction and the transition of STH to mobile holes in β-Ga_2O_3. Hence, carrier generation and recombination mechanisms were found to occur via electron–phonon interaction and STH. The excellent properties of Ga_2O_3 photodetectors pave the way for next-generation high temperature stable solar-blind photodetectors.

ACKNOWLEDGMENTS

B.R.T. and R.S. would like to thank the Department of Physics, IIT Delhi (IITD), for providing XRD facility. We would also like to acknowledge the Nanoscale Research Facility (NRF), IITD, for device fabrication and characterizations. The Department of Science and Technology (DST), India, is highly appreciated for awarding INSPIRE research fellowship to B.R.T. for the Ph.D. programme. The IITD authors acknowledge the NRF project (No. NRF/RP02395) for research support. The KAUST authors are thankful for the support of KAUST baseline fund (No. BAS/1/1664-01-01), KAUST CRG (No. URF/1/3437-01-01), and GCC Research Council (No. REP/1/3189-01-01).

REFERENCES

[1] E. Monroy, F. Omnes, and F. Calle, Semicond. Sci. Technol. **18**, R33 (2003).
[2] L. W. Sang, M. Y. Liao, and M. Sumiya, Sensors **13**, 10482 (2013).
[3] M. Razeghi, Proc. IEEE **90**, 1006 (2002).
[4] W. R. Fahrner, R. Job, and M. Werner, Microsyst. Technol. **7**, 138 (2001).
[5] M. Itzler, S. Donati, M. S. Unlu, and K. Kato, IEEE J. Sel. Top. Quantum Electron. **10**, 665 (2004).
[6] A. BenMoussa, A. Soltani, U. Schuhle, K. Haenen, Y. M. Chong, W. J. Zhang, R. Dahal, J. Y. Lin, H. X. Jiang, H. A. Barkad, B. BenMoussa, D. Bolsee, C. Hermans, U. Kroth, C. Laubis, V. Mortet, J. C. De Jaeger, B. Giordanengo, M. Richter, F. Scholze, and J. F. Hochedez, Diamond Relat. Mater. **18**, 860 (2009).
[7] Z. Alaie, S. M. Nejad, and M. H. Yousefi, Mater. Sci. Semicond. Process. **29**, 16 (2015).
[8] H. So, J. Lim, and D. G. Senesky, IEEE Sens. J. **16**, 3633 (2016).
[9] W. R. Chang, Y. K. Fang, S. F. Ting, Y. S. Tsair, C. N. Chang, C. Y. Lin, and S. F. Chen, IEEE Electron Device Lett. **24**, 565 (2003).
[10] K. W. Liu, M. Sakurai, and M. Aono, Sensors **10**, 8604 (2010).
[11] G. S. Wang, F. Xie, H. Lu, D. J. Chen, R. Zhang, Y. D. Zheng, L. Li, and J. J. Zhou, J. Vacuum Sci. Technol. B **31**, 011202 (2013).
[12] D. M. Brown, E. T. Downey, M. Ghezzo, J. W. Kretchmer, R. J. Saia, Y. S. Liu, J. A. Edmond, G. Gati, J. M. Pimbley, and W. E. Schneider, IEEE Trans. Electron Devices **40**, 325 (1993).
[13] N. Watanabe, T. Kimoto, and J. Suda, Appl. Phys. Express **5**, 094101 (2012).

[14]D. Zhou, F. Liu, H. Lu, D. J. Chen, F. F. Ren, R. Zhang, and Y. D. Zheng, IEEE Photonics Technol. Lett. **26**, 1136 (2014).
[15]A. Hirano, C. Pernot, M. Iwaya, T. Detchprohm, H. Amano, and I. Akasaki, Phys. Status Solidi A **188**, 293 (2001).
[16]J. L. Yang, K. W. Liu, and D. Z. Shen, Chin. Phys. B **26**, 047308 (2017).
[17]M. Orita, H. Ohta, M. Hirano, and H. Hosono, Appl. Phys. Lett. **77**, 4166 (2000).
[18]R. Suzuki, S. Nakagomi, Y. Kokubun, N. Arai, and S. Ohira, Appl. Phys. Lett. **94**, 222102 (2009).
[19]S. H. Lee, S. B. Kim, Y. J. Moon, S. M. Kim, H. J. Jung, M. S. Seo, K. M. Lee, S. K. Kim, and S. W. Lee, ACS Photonics **4**, 2937 (2017).
[20]A. M. Armstrong, M. H. Crawford, A. Jayawardena, A. Ahyi, and S. Dhar, J. Appl. Phys. **119**, 103102 (2016).
[21]D. Y. Guo, Z. P. Wu, P. G. Li, Y. H. An, H. Liu, X. C. Guo, H. Yan, G. F. Wang, C. L. Sun, L. H. Li, and W. H. Tang, Opt. Mater. Express **4**, 1067 (2014).
[22]T. Oshima, T. Okuno, N. Arai, N. Suzuki, S. Ohira, and S. Fujita, Appl. Phys. Express **1**, 011202 (2008).
[23]K. Arora, N. Goel, M. Kumar, and M. Kumar, ACS Photonics **5**, 2391 (2018).
[24]Y. B. Li, T. Tokizono, M. Y. Liao, M. A. Zhong, Y. Koide, I. Yamada, and J. J. Delaunay, Adv. Funct. Mater. **20**, 3972 (2010).
[25]R. Togashi, K. Nomura, C. Eguchi, T. Fukizawa, K. Goto, Q. T. Thieu, H. Murakami, Y. Kumagai, A. Kuramata, S. Yamakoshi, B. Monemar, and A. Koukitu, Jpn. J. Appl. Phys. **54**, 041102 (2015).
[26]D. S. Tsai, W. C. Lien, D. H. Lien, K. M. Chen, M. L. Tsai, D. G. Senesky, Y. C. Yu, A. P. Pisano, and J. H. He, Sci. Rep. **3**, 2628 (2013).
[27]S. Ahn, F. Ren, S. Oh, Y. Jung, J. Kim, M. A. Mastro, J. K. Hite, C. R. Eddy, and S. J. Pearton, J. Vacuum Sci. Technol. B **34**, 041207 (2016).
[28]F. Xie, H. Lu, D. J. Chen, X. L. Ji, F. Yan, R. Zhang, Y. D. Zheng, L. Li, and J. J. Zhou, IEEE Sens. J. **12**, 2086 (2012).
[29]S. Oh, Y. Jung, M. A. Mastro, J. K. Hite, C. R. Eddy, and J. Kim, Opt. Express **23**, 28300 (2015).
[30]T. C. Wei, D. S. Tsai, P. Ravadgar, J. J. Ke, M. L. Tsai, D. H. Lien, C. Y. Huang, R. H. Horng, and J. H. He, IEEE J. Sel. Top. Quantum Electron. **20**, 3802006 (2014).
[31]L. W. Sang, M. Y. Liao, Y. Koide, and M. Sumiya, Appl. Phys. Lett. **99**, 031115 (2011).
[32]H. So and D. G. Senesky, J. Phys. D **49**, 285109 (2016).
[33]B. R. Tak, S. Dewan, A. Goyal, R. Pathak, V. Gupta, A. K. Kapoor, S. Nagarajan, and R. Singh, Appl. Surf. Sci. **465**, 973 (2019).
[34]P. R. Berger, IEEE Potentials **15**, 25 (1996).
[35]D. Zhang, W. Zheng, R. C. Lin, T. T. Li, Z. J. Zhang, and F. Huang, J. Alloys Compd. **735**, 150 (2018).
[36]W. C. Lien, D. S. Tsai, D. H. Lien, D. G. Senesky, J. H. He, and A. P. Pisano, IEEE Electron Device Lett. **33**, 1586 (2012).
[37]S. Oh, C. K. Kim, and J. Kim, ACS Photonics **5**, 1123 (2018).
[38]K. Shimamura, E. G. Villora, T. Ujiie, and K. Aoki, Appl. Phys. Lett. **92**, 201914 (2008).
[39]X. C. Guo, N. H. Hao, D. Y. Guo, Z. P. Wu, Y. H. An, X. L. Chu, L. H. Li, P. G. Li, M. Lei, and W. H. Tang, J. Alloys Compd. **660**, 136 (2016).
[40]B. Zhao, F. Wang, H. Y. Chen, L. X. Zheng, L. X. Su, D. X. Zhao, and X. S. Fang, Adv. Funct. Mater. **27**, 1700264 (2017).
[41]B. Poti, A. Passaseo, M. Lomascolo, R. Cingolani, and M. De Vittorio, Appl. Phys. Lett. **85**, 6083 (2004).
[42]L. Binet and D. Gourier, J. Phys. Chem. Solids **59**, 1241 (1998).
[43]G. Blasse and A. Bril, J. Phys. Chem. Solids **31**, 707 (1970).
[44]T. Harwig and F. Kellendonk, J. Solid State Chem. **24**, 255 (1978).
[45]E. Nogales, B. Mendez, and J. Piqueras, Appl. Phys. Lett. **86**, 113112 (2005).
[46]S. J. Cui, Z. X. Mei, Y. H. Zhang, H. L. Liang, and X. L. Du, Adv. Opt. Mater. **5**, 1700454 (2017).
[47]D. Y. Guo, Z. P. Wu, Y. H. An, X. C. Guo, X. L. Chu, C. L. Sun, L. H. Li, P. G. Li, and W. H. Tang, Appl. Phys. Lett. **105**, 023507 (2014).
[48]M. M. Hou, H. Y. So, A. J. Suria, A. S. Yalamarthy, and D. G. Senesky, IEEE Electron Device Lett. **38**, 56 (2017).
[49]X. Li, J. E. Carey, J. W. Sickler, M. U. Pralle, C. Palsule, and C. J. Vineis, Opt. Express **20**, 5518 (2012).
[50]L. M. B. Vargas, S. de Castro, M. L. Peres, M. P. F. de Godoy, and D. A. W. Soares, J. Alloys Compd. **749**, 734 (2018).
[51]T. Onuma, S. Saito, K. Sasaki, K. Goto, T. Masui, T. Yamaguchi, T. Honda, A. Kuramata, and M. Higashiwaki, Appl. Phys. Lett. **108**, 101904 (2016).
[52]K. Ghosh and U. Singisetti, Appl. Phys. Lett. **109**, 072102 (2016).
[53]A. Y. Polyakov, N. B. Smirnov, I. V. Shchemerov, S. J. Pearton, F. Ren, A. V. Chernykh, P. B. Lagov, and T. V. Kulevoy, APL Mater. **6**, 096102 (2018).
[54]Z. Zhang, E. Farzana, A. R. Arehart, and S. A. Ringel, Appl. Phys. Lett. **108**, 052105 (2016).